The Meteoritical Society

Meteoritics & Planetary Science 43, Nr 1/2, 87–96 (2008)
Abstract available online at http://meteoritics.org

Smelting of Fe-bearing glass during hypervelocity capture in aerogel

Matthew A. MARCUS[1*], Sirine FAKRA[1], Andrew J. WESTPHAL[2], Christopher J. SNEAD[2], Lindsay P. KELLER[3], Anton KEARSLEY[4], and Mark J. BURCHELL[5]

[1]Advanced Light Source, Lawrence Berkeley National Laboratory, Berkeley, California 94720, USA
[2]Space Sciences Laboratory, University of California at Berkeley, Berkeley, California 94720, USA
[3]NASA Johnson Space Center, Houston, Texas 77058, USA
[4]Natural History Museum, London SWY75BD, UK
[5]School of Physical Science, University of Kent, Canterbury, Kent CT2 7NH, UK
*Corresponding author. E-mail: mamarcus@lbl.gov

(Submitted 24 July 2007; revision accepted 31 October 2007)

Abstract–Hypervelocity capture of material in aerogel can expose particles to high transient temperatures. We tested some of the possible effects of capture by using a light-gas gun to shoot particles of basalt glass into aerogel at 6.1 km s^{-1}. Using synchrotron-based micro-X-ray absorption spectroscopy (μXAS), we find that the starting material, in which the Fe was trivalent, is chemically reduced to divalent. In addition, some fragments were chemically reduced so that they contained Fe^0 in a form spectroscopically consistent with a mixture of two forms of iron carbide (cohenite and haxonite). The carbon presumably originated from organic impurities in the aerogel. High-resolution transmission electron microscopy (HRTEM) imaging shows the presence of Fe-rich crystalline nanoparticles. A similar species has been found in actual Stardust material, suggesting that "smelting" effects occurred during capture and should be taken into account when interpreting data on Stardust samples.

INTRODUCTION

The use of aerogel as a capture medium in the Stardust sample return mission (Brownlee et al. 2003) was motivated by the observation that many types of particles can be captured at several km s^{-1} in aerogel and left relatively unaltered (Burchell et al. 2006). Nevertheless, many investigators recognized the potential for alteration of materials due to the severe but very short-lived heating during hypervelocity capture (e.g., Noguchi et al. 2007). However, progress in characterizing this alteration has been slow, principally due to the lack of a suitable homogeneous standard that could be used for reliable and repeatable experiments.

In order to test some effects of aerogel capture, we shot particles of basalt glass into Stardust flight-spare aerogel. Here we report that Fe is reduced from Fe^{3+} to Fe^{2+}, and in many of the fragments, Fe is chemically reduced all the way to Fe^0. This form of Fe^0 is seen in Stardust samples (Fakra et al., unpublished data) as well as in our test samples.

SAMPLES AND EXPERIMENTAL TECHNIQUES

Sample Preparation

The laboratory simulation of impact into aerogel was made using a two stage light-gas gun (Burchell et al. 1999). A sample of powdered basalt glass was used as the projectile. We used NKT-1G basalt glass, supplied by the United States Geological Survey via the Natural History Museum (London). This is a well-characterized sample that was subjected to multiple analyses by several different laboratories (see also http://www.mineralservices.com/s/Laboratory.asp). The nominal analysis (wt%) is approximately 39% SiO_2, 14% MgO, 13% CaO, 13% Fe_2O_3, 10% Al_2O_3, 4% TiO_2, 4% Na_2O, 1% K_2O, 1% P_2O_5, 0.2% MnO. Micro-X-ray absorption spectroscopy (μXAS) analysis (see below) showed that this starting material contained mostly (about two-thirds) trivalent Fe. μXAS spectra on several spots all looked alike, and X-ray fluorescence maps indicated that the composition was uniform. We also found no contribution of Fe^0 (metal, carbide, silicide) in the starting NKT-1G sample. Because Fe^0 species all have a strong signal at energies below where the signal from oxidized Fe starts to rise, we have excellent sensitivity to these species and would detect them at levels far below those quoted below for the aerogel-shot particles. The aerogel target used was flight-spare aerogel manufactured as part of the same batch as the aerogel that was used to fill the Stardust cometary aerogel collector tray (Tsou et al. 2003). This reference provides information on the inorganic and organic impurities in the aerogel.

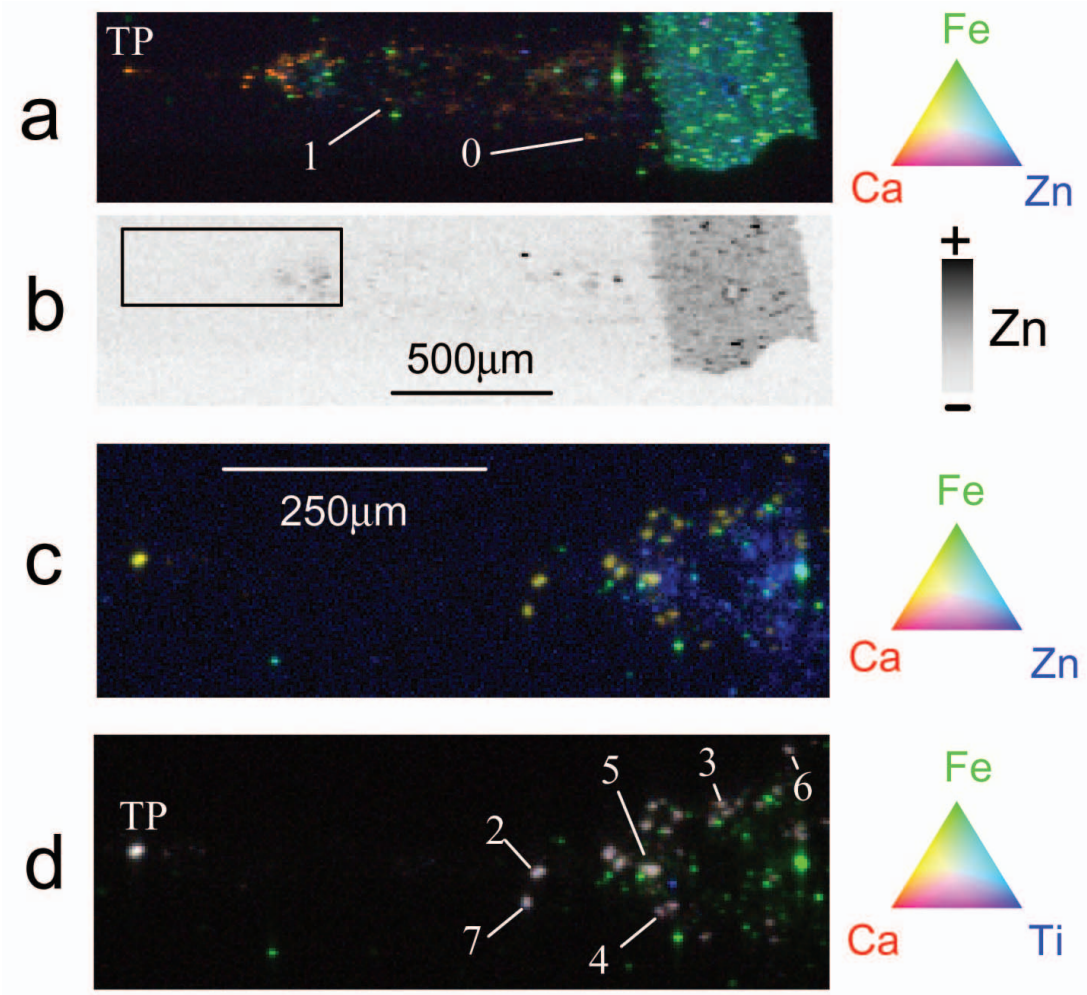

Fig. 1. X-ray fluorescence color coded maps of the basalt-glass track, with Ca, Fe, and Zn or Ti shown in red, green, and blue, respectively, as indicated in the color triangles to the right. The top two images show the coarse maps (10 × 10 μm pixels) of the entire track in the keystone and the two bottom images are fine maps (5 × 5 μm pixels) of an area shown by the black rectangle in (b). The particles on which spectroscopy was performed are called out by numeric labels or "TP," which indicates the terminal particle. b) Negative grayscale map of Zn; note the surface coating of gun residue and the entrance hole. For a discussion of the visual interpretation of tricolor maps, see Manceau et al. (2002).

A cloud of projectiles was fired simultaneously with a mean speed of 6.09 ± 0.13 km s^{-1}. The impacts were at normal incidence in a target chamber at 0.24 mbar pressure. The projectiles used were polydisperse in size, ranging from a few microns to several hundred microns. It has been found (Burchell et al. 2008) that the diameter of the original particle could be estimated as approximately 0.0037 times the length of the resulting track for particles with density near 3 g cm^{-3}. In our case, the track was about 1.9 mm long, so the original projectile would have been ~7 μm in diameter. The entire particle track was extracted from the aerogel tile in a small, wedge-shaped piece of aerogel using the keystoning method developed at the Space Sciences Laboratory, University of California Berkeley (Westphal et al. 2004). The keystone was mounted on a polysilicon microfixture for handling and analysis. The keystone was ~200 μm thick in the direction of the synchrotron X-ray beam.

X-Ray Fluorescence Mapping

In order to locate fragments, we mapped the keystone using micro-X-ray fluorescence (μXRF) on beamline 10.3.2 at the Advanced Light Source, Lawrence Berkeley National Laboratory (Marcus et al. 2004). Elemental mapping was first done with a 16 (horizontal) × 7 (vertical) μm X-ray beam and 10 × 10 μm pixels. On smaller specific regions, we then used a 5 × 5 μm beam and 3 × 3 μm pixels, all at 10 keV incident beam energy.

The light-gas gun produces a spray of Fe-rich particles that mostly stop at the front surface of the aerogel. However, some gun residue enters the track in the wake of the particles being intentionally fired into the aerogel, so it is important to know which Fe-bearing particles are from the test glass. In order to do that, we make use of the compositional homogeneity of the basalt

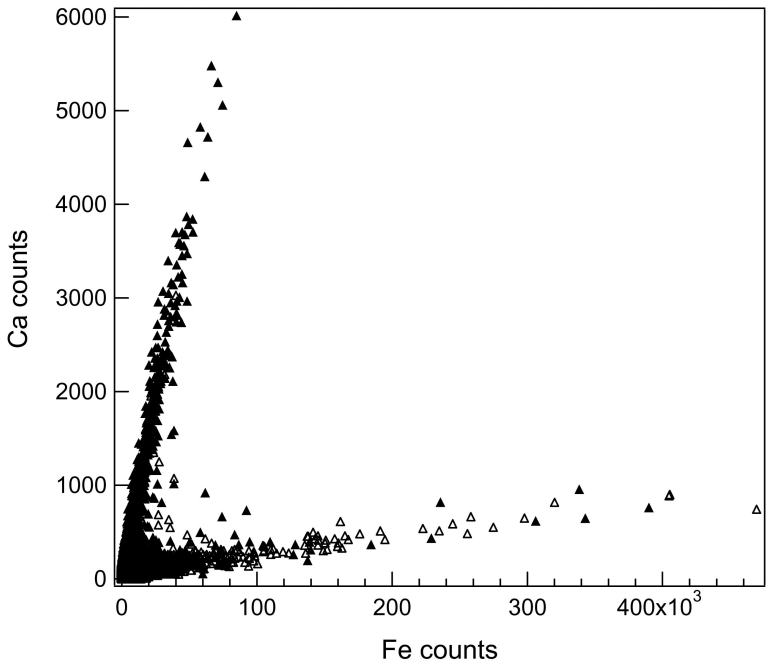

Fig. 2. Fe-Ca pixel-by-pixel scatterplot for the maps shown in Fig. 1. The data for the coarse map (Figs. 1a and 1b) are shown in open triangles and those for the fine maps (Figs. 1c and 1d) in closed triangles. Both maps show two branches, one with a high Fe/Ca ratio (nearly horizontal) indicative of gun residue, and the other with a low and uniform Fe/Ca ratio (nearly vertical) corresponding to basalt glass particles. The ordinate and abscissa are normalized Ca and Fe count rates.

glass. Tricolor maps of the elemental distributions are displayed in Fig. 1.

Particles that are rich in Fe and Zn appear mostly on the surface (green in Figs. 1a–d; black in Fig. 1b, blue in Fig. 1c). Particles that contain Fe, Ca, and Ti in uniform proportions, which is consistent with the basaltic glass projectiles, appear orange-brown in Fig. 1a and white in Fig. 1d. The particles labeled by numbers or "TP" (terminal particle) were examined by μXAS (Manceau et al. 2002) in order to probe the chemical state of Fe. In particular, the presence of Ti is diagnostic since the gun residue does not contain detectable amounts of this element. A pixel-by-pixel scatterplot (Fig. 2) (Manceau et al. 2002) of Fe versus Ca fluorescence shows two branches, one with a low Ca:Fe ratio (ratio of raw counts = 0.0018) and one with a higher ratio (0.072). The latter branch is a straight line showing that all pixels on that branch belong to particles of a constant Ca:Fe ratio, as expected from a uniform projectile. Only particles represented by pixels lying on the high Ca:Fe branch were chosen for spectroscopic study.

Micro X-Ray Absorption Spectroscopy

Once particles were located, we collected Fe K-edge μXAS spectra using an energy range from 100 eV below the edge to 300 eV above. The spot size was 7 × 5 μm or 5 × 5 μm (H × V). We checked the energy calibration using an Fe metal foil (7110.75 eV [Kraft et al. 1996]).

The spectra were deadtime-corrected, pre-edge subtracted and post-edge normalized using a LabView-based software suite available at the beamline (http://xraysweb.lbl.gov/uxas/Beamline/Software/Software.htm). The guiding principle was that X-ray absorption near-edge structure (XANES) spectra of mixtures may be described as linear combinations of spectra from the components (Ressler et al. 2000). We used principal-components analysis (PCA) to see whether the nine spectra could be decomposed into sums of a smaller number of component spectra. We fitted the spectra using a large library of Fe-bearing standards including oxides, oxyhydroxides, basalt glass (oceanic, as described above), indochinite tektites, Fe_3C (from the database of M. Newville; presumably the most common form, cohenite), haxonite (nominally $Fe_{23}C_6$) in a meteoritic specimen from Excalibur Minerals, Fe metal, phyllosilicates, Fe silicides, pyroxenes, amphiboles, olivines, and sulfide minerals. We fitted the spectra by linear least-squares (LSQ) fitting, allowing a small (<0.2 eV) shift of the energy origin and a slight slope to the post-edge background, using a LabView based least-squares fitting program available from the beamline website.

Electron Microscopy

The terminal particle from the keystone was extracted manually using pulled borosilicate glass needles. Excess aerogel was removed and the particle was embedded in Embed 812 and microtomed into 70 nm thick sections, which

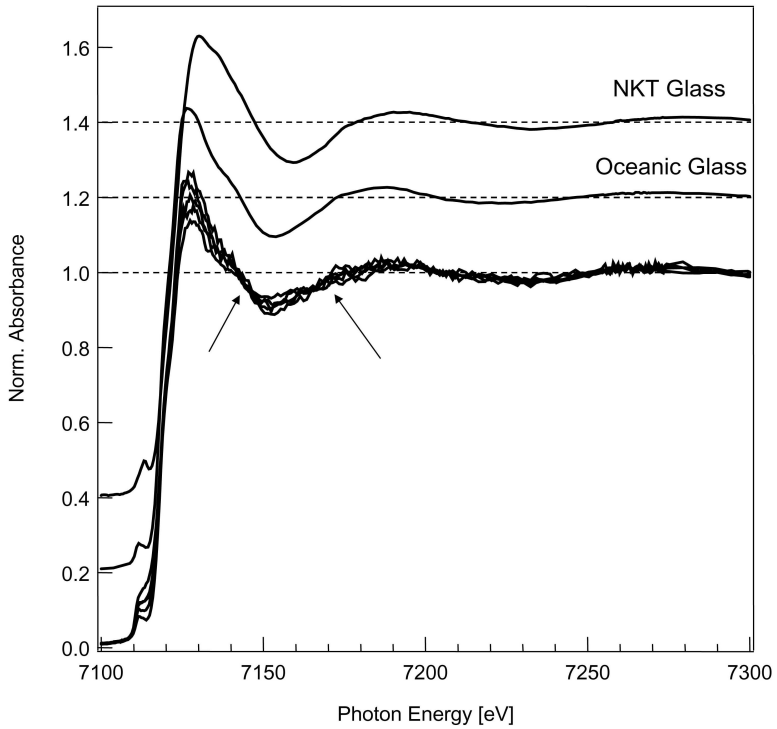

Fig. 3. XANES spectra of five of the nine points (lower curve; four spectra omitted for clarity), the starting (Fe^{3+}-bearing) basalt glass (upper curve) and of oceanic (Fe^{2+}-bearing) basalt glass (middle curve). The dashed lines are the post-edge extrapolated values. The arrows indicate isosbestic points. The tallest peak at the edge belongs to spot 0, followed by 2, 7, 1, and TP, in that order. The pre-edge features follow the same height ordering but in reverse (TP highest, 0 lowest).

were mounted on carbon-coated copper grids. The particles were then examined by high-resolution transmission electron microscopy (HRTEM) using a JEOL 2500SE field emission scanning transmission electron microscope (STEM) at Johnson Space Center's Astromaterials Research and Exploration Science (ARES).

RESULTS AND DISCUSSION

Data Processing and Fitting

For a model glass containing almost exclusively divalent Fe, we used a sample of mid-ocean volcanic basalt glass provided by B. Toner and C. Santelli. It should be noted that this glass was not remelted from crystalline basalt, as was NKT-1G, but solidified as a glass from the liquid. We report that it is this material, not the starting NKT-1G, that best represents what we find in particles in the aerogel. The Fe XANES spectra for both glasses closely resembled what was found in basalt glasses known to be fully reduced (oceanic) and partially oxidized (NKT-1G). The Fe K XANES spectra are shown in Fig. 3 along with those of the two basalt glasses (starting material and oceanic). There is a clear shift of the pre-edge feature and of the main peak between the two glasses. We found no evidence for a contribution from Fe^{3+} in the oceanic glass or in the aerogel-captured particles, as in the starting NKT-1G sample. For clarity, data are shown only out to 7300 eV, though they were collected and fitted up to 7400 eV. The existence of isosbestic points (indicated by arrows) suggests that the nine spectra may be described as weighted sums of just two components. PCA generates a value called *IND*, which depends on the number of components assumed, and which usually is a minimum at the statistically correct number of components (Ressler et al. 2000). In this case, *IND* has a minimum at two components, suggesting that the system is (pseudo)binary. One end-member is indistinguishable from oceanic basalt glass. The TP is at the other end of the series. LSQ fits of all spectra to a three-component system consisting of glass, Fe_3C, and haxonite yield points lying roughly on a straight line on a ternary diagram (Fig. 4; Table 1), again supporting the pseudobinary description. We also fit the data with combinations such as glass-Fe metal-Fe_3C, but none of those fit as well as the glass-Fe_3C-haxonite combination does. X-ray dichroism is a negligible effect in our case because most of the relevant species are cubic or amorphous, and hence not dichroic. Furthermore, TEM indicates that what looks like single particles to the X-ray beam actually consists of many grains, so powder averaging applies even to dichroic species and therefore powder-averaged standards can be used for data analysis.

Figure 5 shows the Ca distribution map of the region displayed in Fig. 1a with the studied particles labeled by their

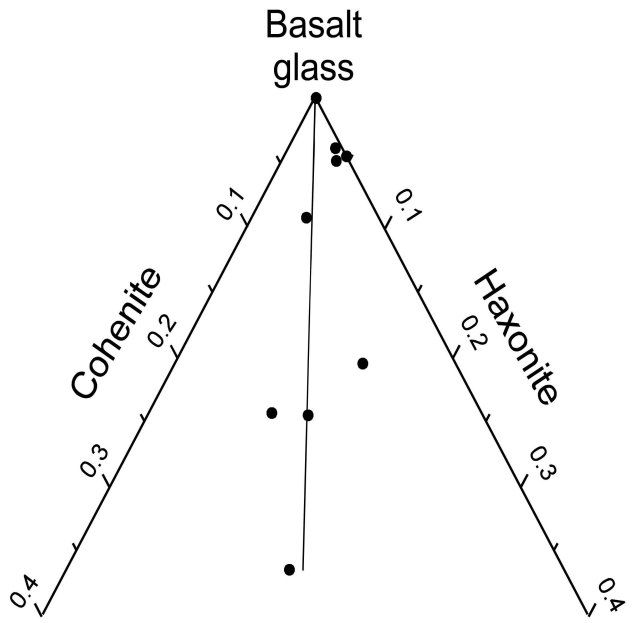

Fig. 4. Fitting results for the spectra of the nine spots to basalt glass (BG), cohenite, and haxonite, shown on a ternary diagram. The numbers on the axes are atom fractions of Fe.

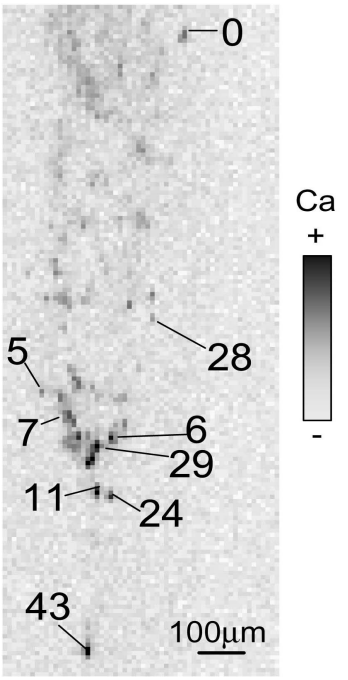

Fig. 5. Micro X-ray fluorescence Ca distribution map of the basalt glass track (shown in negative grayscale using 10 × 10 µm pixels) with the studied spots labeled by their reduced fractions. This map is a section of the one in Fig. 1a.

completely reduced fraction (100% Fe in glass form). We see a general trend of increasing reduction with depth. Because the sample was placed at 45° to the X-ray beam, this map is a projection at an angle to the track, so the position on the image does not directly correspond with the depth below the surface of the aerogel.

TEM

The terminal particle proved to consist of an assemblage of Fe-rich particles in an amorphous matrix that presumably consists of melted aerogel. An HRTEM lattice image of one of these particles is shown in Fig. 6. The dominant lattice fringes are at a distance of 2.15 Å, which is consistent with a strong reflection of haxonite and not of the other species we have considered. In addition, some particles show a *d*-spacing of 2.02 Å, which is consistent with cohenite or metallic Fe.

Interpretation

Our results suggest a two-step reduction process, in which the trivalent Fe in the glass is reduced to divalent in all fragments studied, after which some fragments undergo further reduction to Fe^0. It is possible that the initial reduction occurs due to the melting of particles under vacuum during impact. As shown by Wilke (2005), the Fe^{3+}/Fe^{2+} ratio of a basaltic melt may be adjusted by varying the oxygen fugacity over the melt, so it is plausible that remelting in a vacuum caused reduction of Fe^{3+} to Fe^{2+} (Wilke et al. 2005).

Table 1. Results of linear least-squares fitting of Fe K-edge XANES spectra collected on fragments. Species fractions are in % of Fe atoms in the given form. Error bars on the cohenite and haxonite fractions are ±3%.

Fragment	Glass (%)	Cohenite (%)	Haxonite (%)
0	100	n.d.	n.d.
1	71	18	10
2	89	6	5
3	95	1	6
4	95	1	5
5	71	15	14
6	96	n.d.	5
7	76	8	16
TP	56	23	18

Considering the system to be pseudobinary, we estimated what the Fe XANES spectrum would look like for a fully reduced particle, that is, one with no glass component left in it. We can estimate this spectrum by taking the one for the terminal particle, fitting it to glass plus Fe_3C plus haxonite to derive a fraction of the spectrum to be attributed to glass, then subtracting that fraction of the glass spectrum from the original to get the remaining fraction. The noise quality on the individual TP spectrum is improved if instead we perform these operations on the two-component PCA fit. We thus get an estimate of the spectrum of the end-member of a pseudobinary series whose other end-member is basalt

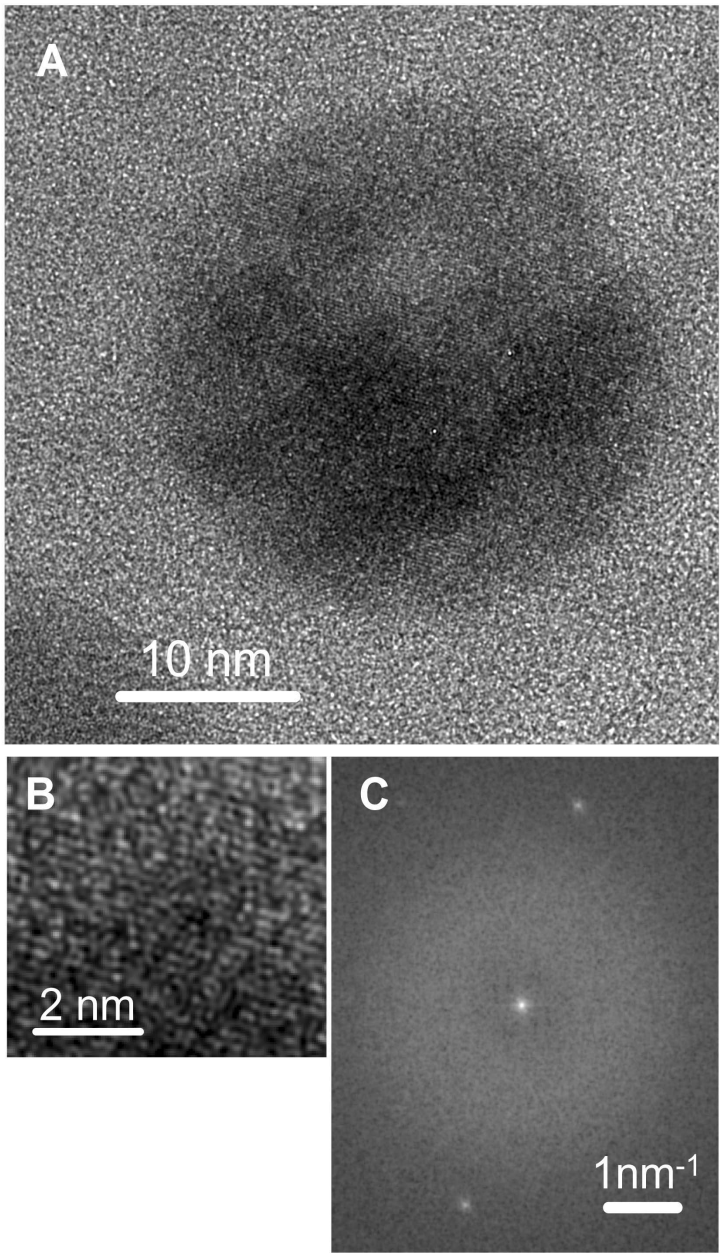

Fig. 6. a) HRTEM image of an Fe-rich grain in the terminal particle. The scale bar is 10 nm. b) Zoomed region in the micrograph, showing lattice fringes. c) Fourier transform magnitude of the top image showing spots corresponding to a *d*-spacing of 2.15 Å, consistent with haxonite.

glass, and which best fits all the data. The result of this series of manipulations is shown in Fig. 7, compared with the spectrum of Fe_3C, haxonite, a best-fit combination of the two and that of a combination of haxonite and FeSi. Adding Fe metal did not improve the fit. In Fig. 8, we show the results of fitting the whole end-member signal to glass plus haxonite, cohenite, Fe, FeSi, or some combination thereof without removing the glass component. This set of fits therefore has one less layer of data manipulation than those in Fig. 7. The fits with the glass and carbide(s) are very good and so in order to make clear the distinction in fit quality between the different fits, we show only the residual, in descending order of goodness of fit. We see that the best fit is obtained using glass, haxonite, and cohenite. Adding positive quantities of Fe or FeSi did not improve the fit.

Since TEM shows that the material is crystalline, such candidates as metallic glassy Fe-C are unlikely contributors. We have checked this by allowing into the fits the spectra of amorphous Fe-C nanoparticles (Cabot, unpublished data; van Wonterghem et al. 1985) and of a commercial Fe-B-Si-C metallic glass (Metglass 2605SC, Metglas, Inc.). No improvement in fit quality is seen, nor do these spectra

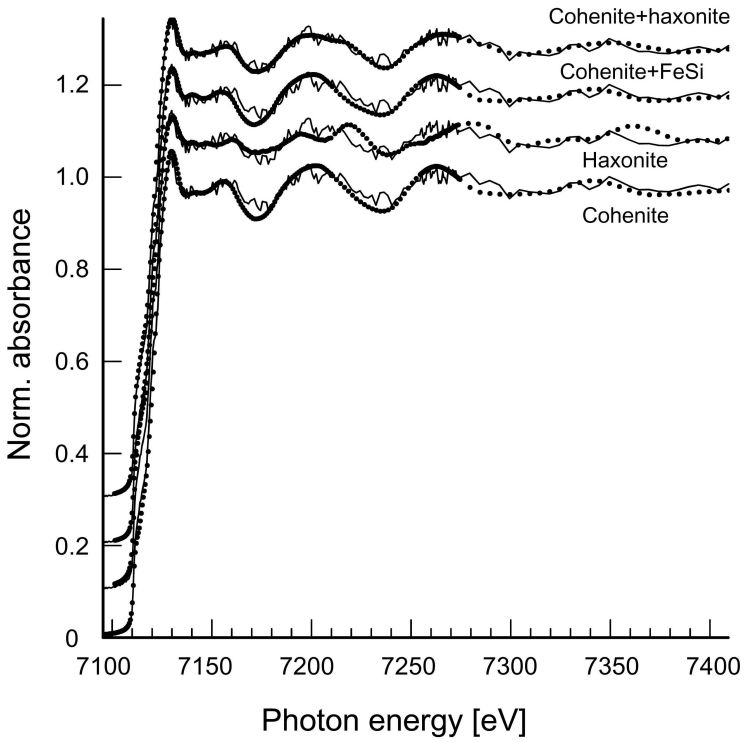

Fig. 7. The inferred "reduced component" compared with fits to Fe carbides and cohenite + FeSi. The addition of Fe or $FeSi_2$ does not improve the fits.

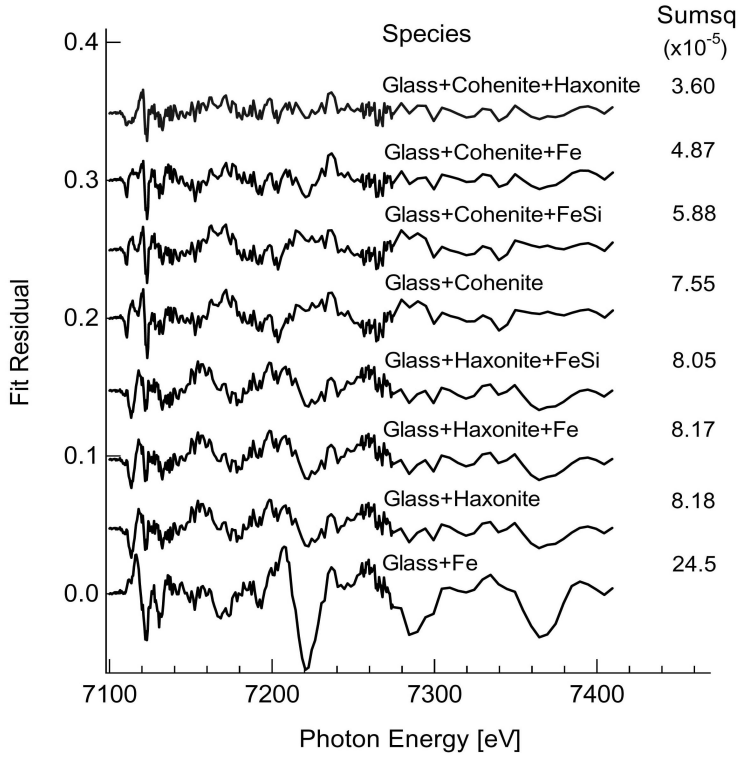

Fig. 8. Fit residuals for the reduced end-member, using basalt glass and various combinations of reduced Fe species as components. The residuals are normalized to a unit edge jump for the original data. The sum square term is defined as the mean-square of the residual divided by the mean-square of the data. The curves are plotted in order of fit quality.

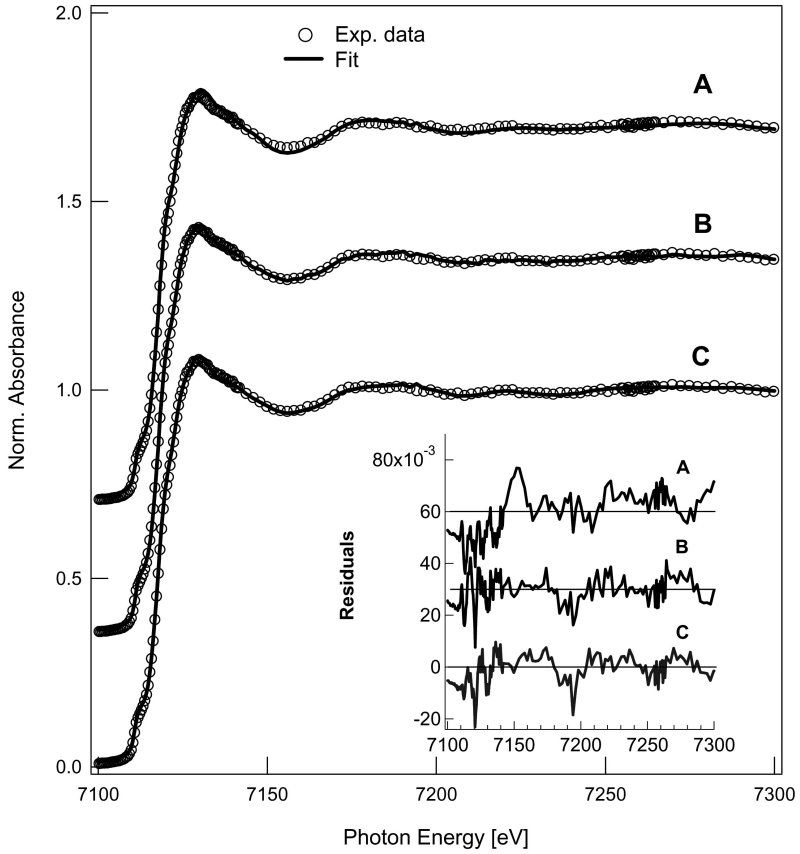

Fig. 9. Track c2052,2,74 particle (dots) and fits. A = awaruite (20%) + FeS (48%) + oceanic glass (31%). B = FeS + TP + Fe. C = FeS + oceanic glass + Fe_3C + Fe. The residuals are shown in the inset. The horizontal lines in the inset show the zero levels for each curve.

resemble our data. Also, we find that FeSi and $FeSi_2$ do not improve the fit quality when added to the list of possible species.

An obvious question to ask is what potential reductant was in the system that could have produced the smelting effect. Since the XANES spectra resemble that of Fe carbides and not any silicide, we must assume carbon as the reductant, which presumably came from organic impurities in the aerogel. While the amount of carbon reported by (Tsou et al. 2003) is small, recent work by Tyliszczak (unpublished data) suggests that the returned aerogel includes up to 8 wt% carbon, so reactions with organics could potentially be important. Similarly, Gallien et al. (2008) found 1–9 wt% carbon in the three samples they studied. There may be a temperature above which the cracked organics are too volatile to remain long enough to react, and below which they are not sufficiently reactive, so that the reaction occurs only over a certain window of entry speeds and particle sizes.

Our results differ from those of Grossemy et al. (2007), who shot a particle of Allende meteorite into aerogel and observed Fe^{3+}-rich particles near the track mouth and Fe^{2+} further in. Their interpretation is that the particle they shot in was olivine, which acquired an oxidized shell on entry. The shell sloughed off as the particle traveled, leaving oxidized material near the track entrance and the original olivine further in. They considered it implausible that any reduction could occur in an environment consisting mostly of oxidized Si. By contrast, we see no evidence for oxidation, but instead find material more reduced than anything in the original material. It may be that olivine is harder to reduce than basalt glass, or that the particular aerogel target we used contained more carbon than theirs.

Another possible interpretation is seen in the work of Davoisne et al. (2006), who deposited a film of amorphous Fe-Ni silicate onto diamond, annealed it in vacuum, and saw the formation of metallic Fe-Ni nanospheres out of the amorphous matrix. They hypothesize that the annealing drove oxygen away from the silicate, leading to an overall reduction. They performed selected-area electron diffraction experiments and reported that the matrix was amorphous. They did not explicitly mention whether the Fe-Ni spheres were amorphous, but given the high annealing temperature, it seems likely that they were crystalline. As we have seen, neither crystalline nor amorphous Fe alone would account for the XANES pattern we see.

An important caveat is that the material tested in this experiment probably is mechanically very different from most of the comet particles. The incident glass projectile was a solid piece of glass, while cometary impactors are probably

friable aggregates of small particles. Thus, it is possible that the heating pulse experienced by the comet particles was not the same as that seen by the test glass particles. Furthermore, it has been found that the loss of S from sulfides in meteoritic samples occurs at varying temperatures, depending on whether the sulfide is a bulk chunk or disseminated through a matrix (Greshake et al. 1998).

The relevance of this experiment to captured Stardust cometary material is illustrated by the data shown in Fig. 9 for a particle in track c2052,2,74. Three fits are shown: A = 20% awaruite + 48% FeS (disordered precipitate) + 31% oceanic glass; B = 51% iron sulfide + 45% basalt-shot terminal particle + 4% Fe metal; and C = 53% FeS + 25% oceanic glass + 15% Fe_3C + 7% Fe metal. As with the aerogel shot, there was no evidence for a significant contribution from oxidized glass. The fit quality with three components, including the reduced basalt, is almost as good as with four components, not including reduced basalt.

CONCLUSIONS

We show evidence for the reduction of Fe^{2+} to Fe^0 under conditions similar to those experienced by mineral grains encountering the Stardust collector. The reaction products are essentially the same for all fragments of the incoming basalt glass particle and have a spectroscopic signature consistent with a mixture of iron carbides and reduced glass. The trend in which the particles furthest from the entry point are more reduced, plus the evidence that carbon is involved, suggests a mechanism in which organics in the aerogel react with the hot incoming particles.

It should be noted that nanophase Fe occurs on the Moon (Keller et al. 1997) and asteroids that have undergone space weathering (Hendrix et al. 2006). However, it is thought that this Fe was reduced by radiation damage and vapor deposition by impacts. The former is not a possibility in our samples, and the latter would produce a fine spray of Fe^0 over the inside of the track, rather than the comparatively large particles we observe. Furthermore, the micro-spectroscopic evidence is not consistent with nanocrystalline Fe, but instead suggests the presence of carbon, supporting the "smelting" hypothesis. Similarly, the mechanisms proposed by both Grossemy et al. (2007) and Davoisne et al. (2006) do not explain our results.

Our work represents a first step toward understanding hypervelocity capture effects on homogeneous glass projectiles. We conclude that the analysis of highly reduced species in Stardust samples must be done carefully, especially since species similar to our reduced basalt were found in actual Wild 2 samples.

Acknowledgments–We gratefully acknowledge the provision of XANES standards by Th. Borch, S. Fendorf, M. Heuer, M. Newville (public database), B. Toner, C. Santelli and A. Cabot. We also gratefully acknowledge discussions with John Bradley. The operations of the Advanced Light Source at Lawrence Berkeley National Laboratory are supported by the Director, Office of Science, Office of Basic Energy Sciences, U.S. Department of Energy under contract number DE-AC02-05CH11231. The Kent light-gas gun operates with a grant from the Particle Physics and Astronomy Research Council (UK).

Editorial Handling—Dr. Christian Koeberl

REFERENCES

Brownlee D. E., Tsou P., Anderson J. D., Hanner M. S., Newburn R. L., Sekanina Z., Clark B. C., Hörz F., Zolensky M. E., Kissel J., McDonnel J. A. M., Sandford S. A., and Tuzzolino A. J. 2003. Stardust: Comet and interstellar dust sample return mission. *Journal of Geophysical Research* 108, doi:10.1029/2003JE002087.

Burchell M. J., Cole M. J., McDonnel J. A. M., and Zarnecki J. C. 1999. Hypervelocity impact studies using the 2 MV Van de Graaff accelerator and two-stage light gas gun of the University of Kent at Canterbury. *Measurement Science and Technology* 10:41–50.

Burchell M. J., Graham G., and Kearsley A. T. 2006. Cosmic dust collection in aerogel. *Annual Reviews of Earth and Planetary Science* 34:385–418.

Burchell M. J., Fairey S. A. J., Wozniakiewicz P., Brownlee D. E., Hörz F., Kearsley A. T., See T. H., Tsou P., Westphal A., Green S. F., Trigo-Rodríguez J. M., and Dominguez G. 2008. Characteristics of cometary dust tracks in Stardust aerogel and laboratory calibrations. *Meteoritics & Planetary Science* 43. This issue.

Davoisne C., Djouadi Z., Leroux H., D'Hendecourt L., Jones A., and Deboffle D. 2006. The origin of GEMS in IDPs as deduced from microstructural evolution of amorphous silicates with annealing. *Astronomy and Astrophysics* 448:L1–L4.

Gallien J.-P., Khodja H., Herzog G. F., Taylor S., Koepsell E., Daghlian C. P., Flynn G. J., Sitnitsky I., Lanzirotti A., Sutton S. R., and Keller L. P. 2008. Characterization of carbon- and nitrogen-rich particle fragments captured from comet 81P/Wild 2. *Meteoritics & Planetary Science* 43. This issue.

Greshake A., Klöck W., Arndt P., Maetz M., Flynn G. J., Bajt S., and Bischoff A. 1998. Heating experiments simulating atmospheric entry heating of micrometeorites: Clues to their parent body sources. *Meteoritics & Planetary Science* 33:267–290.

Grossemy F., Borg J., Djouadi Z., Simionovici A., Lemelle L., Eichert D., Deboffle D., Westphal A. and Snead C. J. 2007. In situ Fe XANES of extraterrestrial grains trapped in aerogel collectors: An analytical test for the interpretation of Stardust samples analyses. *Planetary and Space Science* 55:966–973.

Hendrix A. R. and Vilas F. 2006. The effects of space weathering at UV wavelengths: S-class asteroids. *The Astronomical Journal* 132:1396–1404.

Keller L. P. and McKay D. S. 1997. The nature and origin of rims on lunar soil grains. *Geochimica et Cosmochimica Acta* 61:2331–2341.

Kraft S., Stümpel J., and Kuetgens U. 1996. High-resolution X-ray absorption spectroscopy with absolute energy calibration for the determination of absorption edge energies. *Review of Scientific Instruments* 67:681–687.

Manceau A., Marcus M. A., and Tamura N. 2002 Quantitative

speciation of heavy metals in soils and sediments by synchrotron X-ray techniques. In *Applications of synchrotron radiation in low-temperature geochemistry and environmental science,* edited by Fenter P. A., Rivers M. L., Sturchio N. C., and Sutton S. R. Washington, D.C.: Mineralogical Society of America. pp. 341–428.

Marcus M. A., MacDowell A. A., Celestre R., Manceau A., Miller T., Padmore H. A., and Sublett R. E. 2004. Beamline 10.3.2 at ALS: A hard X-ray microprobe for environmental and materials sciences. *Journal of Synchrotron Radiation* 11:239–247.

Noguchi T., Nakamura T., Okudaira K., Yano H., Sugita S., and Burchell M. J. 2007. Thermal alteration of hydrated minerals during hypervelocity capture to silica aerogel at the fly-by speed of Stardust. *Meteoritics & Planetary Science* 42:357–372.

Ressler T., Wong J., Roos J., and Smith I. 2000. Quantitative speciation of Mn-bearing particulates emitted from autos burning (methylcyclopentadienyl) manganese tricarbonyl-added gasolines using XANES spectroscopy. *Environmental Science and Technology* 34:950–958.

Tsou P., Brownlee D. E., Sandford S. A., Hörz F., and Zolensky M. E. 2003. Wild 2 and interstellar sample collection and Earth return. *Journal of Geophysical Research* 108, doi:10.1029/2003JE002109.

Van Wonterghem J., Mørup S., Charles S. W., Wells S., and Villadsen J. 1985. Formation of a metallic glass by thermal decomposition of $Fe(CO)_5$. *Physical Review Letters* 55:410–413.

Westphal A., Snead C. A., Butterworth A. L., Graham G. A., Bradley J. P., Bajt S., Grant P. G., Bench G., Brennan S., and Pianetta P. 2004. Aerogel keystones: Extraction of complete hypervelocity impact events from aerogel collectors. *Meteoritics & Planetary Science* 39:1375–1386.

Wilke M., Partzsch G. M., Bernhardt R., and Lattard D. 2005. Determination of the iron oxidation state in basaltic glasses using XANES at the K-edge. *Chemical Geology* 220:143–161.